Thermal resistance between low-dimensional nanostructures and semi-infinite media

Matthew A. Panzer[a] and Ken E. Goodson
Department of Mechanical Engineering, Stanford University, Stanford, California 94305, USA

(Received 13 September 2007; accepted 2 February 2008; published online 1 May 2008)

Nanostructured electronic and photonic devices include a high density of material interfaces, which can strongly impede heat conduction and influence performance and reliability. Thermal conduction through interfaces is a very mature discipline for the traditional geometry, in which the lateral interface dimensions are large compared to the phonon wavelength. In nanostructures, however, the localization of phonons in the directions parallel to the interface may strongly influence the effective thermal resistance. The present work investigates model problems of abrupt junctions between a harmonic one-dimensional (1D) and a three-dimensional (3D) fcc lattice and between a 1D and a two-dimensional square lattice. The abrupt change in geometry modifies the phonon modes participating in energy transmission and creates an additional thermal resistance that is comparable with that occurring due to the acoustic mismatch at the interface of bulk media. For both cases, varying the impedance mismatch at the junction suggests that engineering an intentional impedance mismatch at a nanostructured interface may enhance the transmission of energy. The lattice dynamics calculations are used to develop qualitative arguments for the interface resistances in the practical geometries involving carbon nanotubes, silicon nanopillars, and graphene. This research provides foundations for detailed investigations of the impact of localized phonon modes on the acoustic mismatch resistance. © *2008 American Institute of Physics*. [DOI: 10.1063/1.2903519]

I. INTRODUCTION

Nanostructured electronic and photonic devices typically contain materials with nanoscale dimensions that interface with larger micro- or macrostructures at scales comparable to the phonon wavelength. These abrupt junctions between materials with differing dimensionality often arise because of the need to interface the nanosystem with the macroenvironment or thermal reservoirs. Examples of such geometry include recent experimental work measuring localized heating as a function of length of a single hydrocarbon molecule bonded between two electrodes,[1] or the use of microfabricated suspended bridges coupled to large cavities for studying the quantized nature of thermal conductance.[2] Similarly, suspending an isolated carbon nanotube between two reservoirs is a common technique to study its thermal and electrical properties. This measurement geometry has yielded a variety of data such as thermal and electrical conductivities[3–5] as well as shown interesting properties such as thermal rectification arising from nonlinear contact effects.[6] Recent experimental work on bulk arrays of aligned carbon nanotubes for thermal management applications revealed that nanoscale contact effects significantly reduce the thermal performance of the nanotube structures.[7,8]

Low temperature phonon transport through three-dimensional (3D) point contacts ranging in scale from a few nanometers to 1000 nm was reviewed by Feher *et al.*[9] In addition to the emergence of size and ballistic transport effects for contact dimensions less than 1000 nm, the work discussed the emergence of phonon diffraction effects on thermal transport through nanoscale contacts (~100 nm) at low temperatures ($T \sim 1$ K).[10,11] For contact dimensions less than 10 nm, this work highlighted the impact of the crystal geometry and surface effects in modifying the phonon spectral densities. In particular, the work demonstrated the modification in local phonon density of states for atoms located on the center plane of square atomic bridge structures with fcc crystal structure and edge lengths of 6 and 12 lattice constants bridging semi-infinite fcc crystals. The consequences of the modified phonon states on the thermal resistances in the structure were left unexplored.

Previous work modeling the thermal transport through abrupt nanoscale contacts has employed both continuum mechanics approaches and atomistic simulations. Research specifically focusing on the phonon transmission through an abrupt junction has extensively relied on continuum mechanics approaches, which are valid in the long wavelength limit and which normally apply at low temperatures. In this approach, the energy transmission through the junction is typically computed through a Green's function solution of the continuum equations of motion across the junction. Angelescu *et al.*[12] analyzed the energy transmission coefficient for an abrupt junction between two continuum two-dimensional (2D) rectangular media by applying scalar wave mechanics with fixed boundaries, letting the width of one cavity tend to infinity. Cross and Lifshitz[13] analyzed the same geometry but assumed a more realistic stress-free boundary condition on all free surfaces, predicting a linear scaling of the transmission coefficient with frequency for all transverse bridge modes. The work also analyzed the junction using a long wavelength approximation to the full vector mechanics theory, which included the contributions of local-

[a]Electronic mail: mpanzer@stanford.edu.

ized Rayleigh-like surface states to the energy transmission. Continuum analysis in full scalar and long wavelength perturbative vector approaches with stress-free boundary conditions has also been extended to 3D abrupt junctions in rectangular[14] and cylindrical geometries.[15] The prior continuum work suggests that the free surface created at an abrupt junction can significantly alter phonon modes that participate in heat transfer, creating additional contributions to the thermal resistance of the structure.

Atomistic modeling approaches provide a more detailed framework to model transport in nanostructures and directly include quantum effects. The majority of atomistic modeling of nanoscale interfaces has focused on computing the energy transmission through a one-dimensional (1D) atomic lattice linking two thermal reservoirs.[16–20] The simulations provide a detailed analysis of the transport physics through the atomic structure, but typically employ approximations to incorporate the effect of the reservoir contact on energy transmission through the structure. For example, Ohtsubot *et al.*[16] used classic molecular dynamics simulations to investigate the energy transmission through a 1D atomic lattice by approximating the reservoir contacts as adiabatic.

The study of quantum transport through atomic structures using Hamiltonian and Green's function techniques has incorporated more rigorous modeling of the contact physics. Approximation techniques to incorporate reservoir interface effects have included using the Debye density of state approximation within the Landauer formalism,[17] the continuum-based local surface density of states (LDOS) in the Hamiltonian[18] and nonequilibrium Green's function formalism,[20] and a finite extension of the atomic structure into the reservoir using the Hamiltonian formalism.[19] Incorporating the dynamics of the reservoir as a finite extension of the atomic system[19] showed significant impact on phonon transport through the system such as reduced transmission of transverse phonon modes. However, the computational constraints on the size reservoir domain limited its dimension to scales comparable to the phonon wavelength, which may inadequately capture the entire impact of the reservoir dynamics. Similarly, the LDOS approximation based on continuum theory may be inadequate to represent the true LDOS of an atomic contact, particularly for higher frequency phonon modes.

The prior atomic scale and continuum modeling indicates that the details of the reservoir dynamics modify the energy transmission in nanoscale structures. Rigorous modeling of phonon transmission through an abrupt nanoscale contact presents a multiscale computational challenge, requiring detailed analysis of an atomic scale structure connected to a macroscale reservoir.

This work uses a lattice dynamics calculation between a 1D harmonic lattice and a 3D fcc lattice, and between a 1D and a 2D square lattice to provide perspective on the impact of phonon reservoir modes on thermal transport through an abrupt nanoscale junction. The lattice dynamics approach to predicting thermal boundary resistances has been applied to a variety of interfaces between lattices of similar dimensionality.[21,22] To our knowledge, it has not been applied to the prediction of interface resistances between lattices of differing dimensionality. The approach presented here provides a rigorous solution of the lattice dynamics in this simplified model for an atomic point contact at all phonon wavelengths, within the assumptions of the model. We use the simplified geometry studied here to discuss the qualitative behavior of thermal transport through more practical geometries involving carbon nanotubes, silicon nanopillars, and graphene.

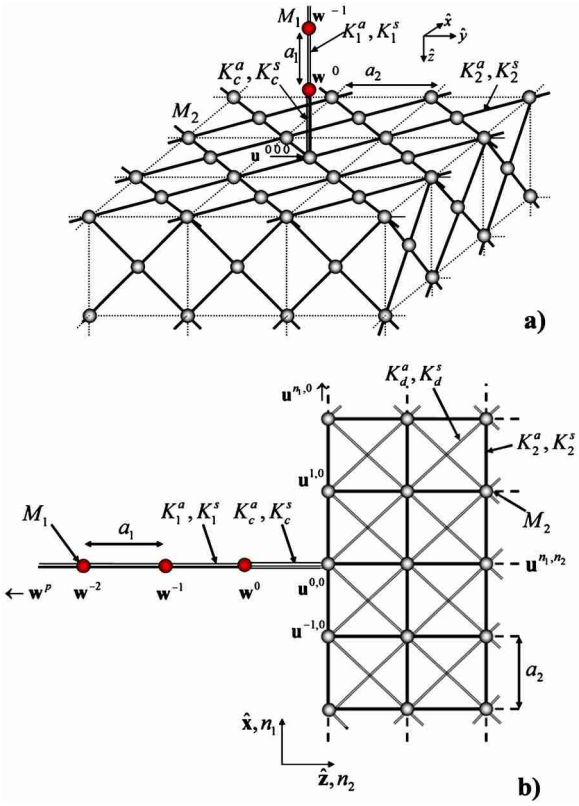

FIG. 1. (Color online) Schematic illustration of the lattice geometry used in this study. (a) Junction between a 1D lattice and the (001) surface of semi-infinite fcc lattice extending in the positive z direction. (b) Junction between 1D lattice and the (01) surface of a semi-infinite 2D square lattice extending in the positive z direction.

II. MODEL

This work uses a lattice dynamics analysis to investigate the phonon transmission through the two junctions geometries depicted in Fig. 1. In the first case, a 1D harmonic lattice is bonded to an individual atom on the (001) surface of a semi-infinite fcc lattice extending in the positive z direction with nearest-neighbor harmonic interactions. The mass of the atoms in the fcc lattice is M_2 and they interact through the nearest-neighbor axial (K_2^a) and shear (K_2^s) stiffnesses. In the second case, the 1D lattice bonds to the (01) surface of a 2D square lattice with second nearest-neighbor harmonic interactions. For the two-dimensional lattice, we consider atomic motion confined to the plane with nearest-neighbor axial and shear stiffnesses (K_2^a, K_2^s) and second nearest-neighbor axial and shear stiffnesses (K_d^a, K_d^s) along the unit cell diagonal. In the 1D lattice, we consider nearest-neighbor interactions between the atoms with mass M_1, characterized by axial and shear (K_1^a, K_1^s) bond stiffnesses. At the interface

contact, the lattices interact through a nearest-neighbor interaction with axial and shear (K_c^a, K_c^s) bond stiffness constants, which can potentially differ from those in either of the bulk domains. We choose values for the bond parameters that yield the Lamé constants in the continuum limit[23] of the 2D lattice. To simplify the analysis, we neglect the bond torsion stiffness, assume that equilibrium positions of the atoms near the interface retain the bulk lattice structure (see Ref. 24 for discussion of surface structure modification effects), and assume that there are no foreign species bonded on the interface surface. Because the linear elastic continuum equations of motion (see Ref. 25) for a medium couple the displacement field components, consistency between the 2D square lattice and its continuum limit motivates the need to include second nearest-neighbor interactions for this lattice.

From the perspective of the semi-infinite lattice, the phonon mode incident from the 1D domain appears as a localized steady periodic source radiating at the surface. The response of an elastic continuum half-space to either a point source or line source was first studied by Lamb.[26] Others have studied finite radiating sources of various geometries.[27–30] In general, the effect of a localized radiating surface source is to produce an excitation composed of a superposition of bulk modes that is highly localized along the free interface. The continuum mechanics analogy with the pointlike surface interaction in this work suggests that the modes in the 1D lattice will couple strongly to a superposition of modes in the semi-infinite lattice that are localized near the surface. Consequently, the local density of states of the atomic point contact with the discrete lattice is expected to differ from both the bulk density of states and the continuum free-surface approximation to the local density of states. The modification in the LDOS will affect the energy transmission and thermal conductance of the interface. In particular, the transmission coefficient will be less than unity, even for a junction between materials with identical bulk lattice properties.

We calculate the phonon transmission using Green's function approach as follows. We first solve for Green's function for the response of the semi-infinite lattice to a harmonic point force on the surface, and then find the coupling of that force to the 1D lattice modes. The first step in computing surface Green's function is to find the bulk eigenmodes in the semi-infinite lattice and their associated dispersion relation for a given frequency ω. The equations of motion for surface atoms in response to harmonic forces spatially distributed along the surface with arbitrary spatial frequency provide boundary conditions to be satisfied by a superposition of bulk modes. Then, an appropriate superposition of these solutions yields the response of the semi-infinite lattice to a harmonic point force of frequency ω localized on the atom at the index origin, $(n_1,n_2,n_3)=(0,0,0)$. The boundary conditions of the junction relate this point force to the 1D lattice dynamics to determine the amplitude ratios of the reflected modes in the 1D lattice and the transmitted modes in the semi-infinite lattice to the incident mode in the 1D lattice. The difference between the energy of the incident wave and the reflected wave is the energy that is transmitted across the interface, which gives the frequency dependent transmission coefficient of the junction.

A. Surface Green's function for semi-infinite lattice

Prior research investigating the dynamics of semi-infinite lattices has considered 1D lattices,[31] 2D square lattices with second nearest-neighbor interactions,[23] 2D hexagonal lattices,[32] and 3D lattices.[33,34] In this section, we present our formulation for constructing surface Green's function for the semi-infinite fcc lattice. The 2D case follows an analogous approach and the details for computing the lattice dynamics of a square lattice with second nearest-neighbor interaction and finite extent were studied by Suiker.[23] Because our analysis of a semi-infinite 2D domain differs mainly in the boundary conditions, we will refer the reader to Ref. 23 for the details of the calculations for the 2D case.

We represent the atomic displacement of the atoms in the fcc lattice by $\mathbf{u}^{n_1,n_2,n_3}$ for the atom located at $\mathbf{R}=n_1\mathbf{a}_1+n_2\mathbf{a}_2+n_3\mathbf{a}_3$, where the primitive lattice vectors are

$$\mathbf{a}_1=\frac{a_2}{2}(\hat{\mathbf{y}}+\hat{\mathbf{z}}),\quad \mathbf{a}_2=\frac{a_2}{2}(\hat{\mathbf{z}}+\hat{\mathbf{x}}),\quad \mathbf{a}_3=\frac{a_2}{2}(\hat{\mathbf{x}}+\hat{\mathbf{y}}), \tag{1}$$

and where a_2 is the lattice constant of the conventional cell. The equations of motion are

$$M_2\ddot{\mathbf{u}}^{n_1,n_2,n_3}=-\frac{\partial U}{\partial \mathbf{u}^{n_1,n_2,n_3}}, \tag{2}$$

where U is the crystal potential energy. For harmonic nearest-neighbor axial (K_2^a) and shear stiffness (K_2^s) interactions, U is given by

$$U=\sum_{m_1,m_2,m_3=n.n.}\frac{1}{2}K_2^a(\Delta\mathbf{l}^{m_1,m_2,m_3})^2+\frac{1}{2}K_2^s(\Delta\mathbf{s}^{m_1,m_2,m_3})^2, \tag{3}$$

where the sum runs over the indices of the nearest neighbors of the atom located at (n_1,n_2,n_3) and where $\Delta\mathbf{l}^{m_1,m_2,m_3}$ and $\Delta\mathbf{s}^{m_1,m_2,m_3}$ are the interatomic axial stretch and shear displacements that are given by

$$(\Delta\mathbf{l}^{m_1,m_2,m_3})^2=[(\mathbf{u}^{m_1,m_2,m_3}-\mathbf{u}^{n_1,n_2,n_3})\cdot\hat{\mathbf{d}}^{m_1,m_2,m_3}]^2, \tag{4}$$

$$(\Delta\mathbf{s}^{m_1,m_2,m_3})^2=(\mathbf{u}^{m_1,m_2,m_3}-\mathbf{u}^{n_1,n_2,n_3})^2-[(\mathbf{u}^{m_1,m_2,m_3}-\mathbf{u}^{n_1,n_2,n_3})\cdot\hat{\mathbf{d}}^{m_1,m_2,m_3}]^2, \tag{5}$$

where $\hat{\mathbf{d}}^{m_1,m_2,m_3}$ is unit vector along the interatomic bond direction. Equation (2) is solved by assuming a solution of the form

$$\mathbf{u}_j^{n_1,n_2,n_3}=\mathbf{C}_j e^{i(\mathbf{R}\cdot\mathbf{k}_j-\omega t)}, \tag{6}$$

where

$$\mathbf{R}\cdot\mathbf{k}_j=\frac{a_2}{2}[(n_2+n_3)k_x+(n_1+n_3)k_y+(n_1+n_2)k_{z,j}]=\mathbf{R}\cdot(\mathbf{k}_\parallel+k_{z,j}\hat{\mathbf{z}}), \tag{7}$$

where $\mathbf{C}_j$ are the Cartesian displacement amplitude compo-

nents and k_x, k_y, and $k_{z,j}$ are the Cartesian components of the wavevector. We denote the projection of the wavevector $\mathbf{k}$, on the plane of the free interface as $\mathbf{k}_\parallel$ and the component in the semi-infinite direction as $k_{z,j}$. The subscript j labels the three degenerate solutions that will arise from the solution of Eq. (2) for a given choice of $\mathbf{k}$ and ω, corresponding to generalized longitudinal and transverse waves. In general, the presence of the free interface will cause $k_{z,j}$ to be complex valued.

Substituting Eq. (6) into Eq. (2) yields the following three by three system of equations whose solution gives the dispersion relation and amplitude component ratio for the three degenerate bulk modes,

$$[M_2\omega^2\mathbf{I}+\mathbf{D}]\mathbf{C}_j=\mathbf{0}, \tag{8}$$

where

$$D_{11}=4K_2^a(bc_j-1)+4\left(\frac{K_2^n+K_2^s}{2}\right)(ab+ac_j-2), \tag{9}$$

$$D_{22}=4K_2^s(ac_j-1)+4\left(\frac{K_2^a+K_2^s}{2}\right)(bc_j+ab-2), \tag{10}$$

$$D_{33}=4K_2^s(ba-1)+4\left(\frac{K_2^a+K_2^s}{2}\right)(bc_j+ac_j-2), \tag{11}$$

$$D_{12}=D_{21}=-4\left(\frac{K_2^a-K_2^s}{2}\right)\left[\sin\left(\frac{k_xa_2}{2}\right)\sin\left(\frac{k_ya_2}{2}\right)\right], \tag{12}$$

$$D_{13}=D_{31}=-4\left(\frac{K_2^a-K_2^s}{2}\right)\left[\sin\left(\frac{k_xa_2}{2}\right)\sin\left(\frac{k_{z,j}a_2}{2}\right)\right], \tag{13}$$

$$D_{23}=D_{32}=-4\left(\frac{K_2^a-K_2^s}{2}\right)\left[\sin\left(\frac{k_ya_2}{2}\right)\sin\left(\frac{k_{z,j}a_2}{2}\right)\right], \tag{14}$$

where

$$a=\cos\left(\frac{k_xa_2}{2}\right),\quad b=\cos\left(\frac{k_ya_2}{2}\right),\quad c_j=\cos\left(\frac{k_{z,j}a_2}{2}\right). \tag{15}$$

Since the Fourier space approach to constructing surface Green's function requires superposing the bulk modes to solve for the response of the half-space to a periodic surface force with the in-plane wavevector $\mathbf{k}_\parallel$ and frequency ω, it is convenient to take the determinant of Eq. (8) and solve for $k_{z,j}$ in terms of $\mathbf{k}_\parallel$ and ω to yield explicit relations for bulk displacement fields [Eq. (6)] in terms of these variables. Taking the determinant of Eq. (8) and solving for $k_{z,j}$ yield an explicit third order polynomial in c_j. The subscript j indexes the three roots of this polynomial, which lead to six values of $k_{z,j}$ corresponding to

$$k_{z,j}=\pm\frac{2}{a_2}\arccos(c_j). \tag{16}$$

In analyzing energy transmission into the semi-infinite lattice from the localized surface excitation, we will apply the radiation boundary condition in which we choose the wavevectors that correspond to modes that carry energy away from interface and are finite in the positive z direction. Because $k_{z,j}$ are in general complex valued, this boundary condition requires that the three physically acceptable solutions to Eq. (16) have positive imaginary components. With $k_{z,j}$ in terms of $\mathbf{k}_\parallel$ and ω, solving Eq. (8) for the ratio of the x and y to z components of the three bulk modes gives

$$\chi_{xj}=\frac{C_{x,j}}{C_{z,j}}=-\frac{[D_{23}(D_{11}+M_2\omega^2)-D_{13}D_{21}]}{[D_{22}(D_{11}+M_2\omega^2)-D_{21}^2]}, \tag{17}$$

$$\chi_{yj}=\frac{C_{y,j}}{C_{z,j}}=-\frac{(D_{13}(D_{22}+M_2\omega^2)-D_{23}D_{12})}{(D_{22}(D_{11}+M_2\omega^2)-D_{21}^2)}, \tag{18}$$

$$\chi_{zj}=1. \tag{19}$$

The next step to constructing surface Green's function is to compute the response of the lattice to a harmonic surface force with spatial frequency $\mathbf{k}_\parallel$. The equations of motion for the atoms at the surface provide boundary conditions, which are satisfied by a superposition of the degenerate bulk modes at frequency ω. Then, an appropriate superposition of the response of the semi-infinite lattice to a spatially periodic force will yield the response of the semi-infinite lattice to a temporally harmonic point force located at $(n_1,n_2,n_3)=(0,0,0)$. The equations of motion for the surface atoms are

$$M_2\ddot{\mathbf{u}}^{n_1,n_2,n_3}=-\frac{\partial U_s}{\partial\mathbf{u}^{n_1,n_2,n_3}}+\mathbf{F}^{n_1,n_2,n_3}, \tag{20}$$

where $\mathbf{F}^{n_1,n_2,n_3}$ is the external force acting on the surface atom at (n_1,n_2,n_3), U_s is the potential energy for an atom on the (001) surface, and (n_1,n_2,n_3) are restricted to surface sites. Assuming that the lattice retains its bulk structure and bond stiffnesses at the surface, and that there are no interactions arising from the negative z half-space, the potential energy for atoms on the surface sites, U_s, is

$$U_s=\sum_{m_1,m_2,m_3=n.n.z\geq 0}\frac{1}{2}K_2^a(\Delta\mathbf{l}^{m_1,m_2,m_3})^2+\frac{1}{2}K_2^s(\Delta\mathbf{s}^{m_1,m_2,m_3})^2, \tag{21}$$

where the sum runs only over atoms with positions on the surface and in the positive z direction. We assume a force distributed along surface of the form

$$\mathbf{F}^{n_1,n_2,n_3}=\mathbf{f}(\mathbf{k}_\parallel)e^{i(\mathbf{k}_\parallel\cdot\mathbf{R}-\omega t)}, \tag{22}$$

where $\mathbf{R}$ is confined to surface and $\mathbf{f}$ is the amplitude of the force. We seek a solution to Eq. (20) that is a superposition of the three degenerate bulk modes with wavevector $\mathbf{k}_\parallel$ and frequency ω,

$$u_i^{n_1,n_2,n_3}(\mathbf{k}_\parallel) = \left\{ \sum_{j=1}^{3} A_j \chi_{ij} e^{i[k_{z,j} a_2/2(n_1+n_2)]} \right\} e^{i(\mathbf{k}_\parallel \cdot \mathbf{R} - \omega t)}, \quad (23)$$

where A_j are the amplitude coefficients of each of the three degenerate bulk modes. Substituting Eqs. (22) and (23) into Eq. (20) gives a three by three system of equations to be solved for the amplitude coefficients, A_j,

$$\mathbf{HA} = -\mathbf{f}, \quad H_{ij} = \chi_{ij} M_2 \omega^2 - \left[\frac{\partial U_s}{\partial u_i^{n_1,n_2,n_3}} \right]_j, \quad (24)$$

where the last term is interpreted as individually evaluating the ith component of the gradient of the interatomic potential for a surface atom with respect to $\mathbf{u}^{n_1,n_2,n_3}$ with the jth term in Eq. (23). Then, we can construct a force localized on the atom at $(n_1,n_2,n_3)=(0,0,0)$, namely, $F_i^{n_1,n_2,n_3} = F_i \delta_{n_1,0} \delta_{n_2 0} \delta_{n_3,0}$, where F_i is the magnitude of the ith component of the force acting on the atom at (0,0,0) and $\delta_{n_i,0}$ is the Kronecker delta, by choosing the Fourier components of Eq. (22) to be $f_i(\mathbf{k}_\parallel)=F_i$ and integrating Eq. (23) over the 2D (001) surface Brillouin zone with a density of states of $A_{\text{cell}}/(2\pi)^2$, where A_{cell} is the direct-space area of the (001) surface unit cell. Superposing the Fourier space solutions, the total displacement amplitude for the point force is then given by

$$\mathbf{u}^{n_1,n_2,n_3} = \iint_{(001)b.z.} \frac{A_{\text{cell}}}{(2\pi)^2} \mathbf{u}^{n_1,n_2,n_3}(\mathbf{k}_\parallel) d\mathbf{k}_\parallel. \quad (25)$$

In calculating the energy transmission to the semi-infinite lattice, we assume that the 1D lattice only interacts with the displacement of the atom located at (0,0,0), which simplifies Eq. (25) to only evaluating the $(n_1,n_2,n_3)=(0,0,0)$ term. Thus, the displacement of the atom at the origin of the semi-infinite lattice is related to the external force ($\mathbf{F}$) on that atom by

$$\mathbf{u}^{0,0,0} = \mathbf{GF}, \quad (26)$$

with

$$\mathbf{G} \equiv -\iint_{(001)b.z.} \frac{A_{\text{cell}}}{(2\pi)^2} \boldsymbol{\chi} \mathbf{H}^{-1} d\mathbf{k}_\parallel. \quad (27)$$

When evaluating the integral in Eq. (27), we causally perturb the vibration frequencies to $\omega^2 \rightarrow \omega^2 + i\delta$ in the limit as $\delta \rightarrow 0^+$, where δ is a small number that related to the energy resolution of $\mathbf{G}$ and whose physical significance is discussed in Ref. 35. We use δ of the form recommended by Ref. 36, specifically

$$\delta = 0.02\left(1 - \frac{\omega}{\omega_{\max}}\right)\omega^2, \quad (28)$$

where $\omega_{\max}$ is the maximum lattice vibration frequency. Smaller values of δ increase the energy resolution at the expense of computational time. Physically, $\mathbf{G}$ can be interpreted as Green's function for a surface atom since G_{ij} represents the displacement in the ith direction of a surface atom in response to a localized force on that atom in the jth direction. Due to the appearance of $\mathbf{H}^{-1}$ in Eq. (27), large contributions to the integral arise from wavevector with $\mathbf{k}_\parallel$ such that $\det(\mathbf{H}) \sim 0$, which, in light of Eq. (24), occurs when there is near zero surface force. This condition is equivalent to free-surface modes, which are localized near the interface, analogous to Rayleigh surface waves in the continuum,[25] indicating that these localized modes strongly contribute in the phonon coupling from the 1D lattice to the semi-infinite lattice.

Symmetry of the equations of motion under the transformation $x \leftrightarrow y$ implies that $G_{xx}=G_{yy}$ and $G_{xz}=G_{yz}$. Mirror symmetry about the x and y axes implies that $G_{xy}=G_{yx}=G_{xz}=G_{yz}=0$, which numerical evaluation of $\mathbf{G}$ confirmed. Similarly, numerical evaluation $\mathbf{G}$ shows that $|G_{zx}|, |G_{zy}| \ll |G_{xx}|, |G_{zz}|$ for all frequencies, indicating that the in-plane forces weakly couple to normal displacements of the surface. Consequently, the reflection of energy from a longitudinal polarization incident from the 1D lattice into transverse polarizations is weak, and similarly for energy reflected from transverse polarization incident from the 1D lattice into longitudinal polarizations. The LDOS, ρ, for an atomic site on the surface the surface is related to Green's function through the relation[36,37]

$$\boldsymbol{\rho} = \frac{-M_2 2\omega}{\pi} \lim_{\delta \rightarrow 0^+} \{-\text{Im}[\mathbf{G}(\omega^2 + i\delta)]\}, \quad (29)$$

where the additional negative sign arises due to our sign convention in defining Green's function, and the mass factor from our definition of the dynamic matrix. We verified the calculation by comparing the form of the local density of states to that of palladium[37] and by comparing the numerical evaluation of $\mathbf{G}$ for the 2D lattice in the low frequency limit with the analogous continuum solution given in Ewing *et al.*[30]

B. Energy transmission between the 1D and semi-infinite lattices

The interaction of the semi-infinite lattice with the 1D lattice through the coupling constants K_c^a and K_c^s (Fig. 1) gives the forces F_i imposed on the semi-infinite lattices

$$\mathbf{F} = \mathbf{S}_c(\mathbf{w}^0 - \mathbf{u}^{0,0,0}), \quad \mathbf{S}_c = \begin{bmatrix} K_c^s & & \\ & K_c^s & \\ & & K_c^a \end{bmatrix}, \quad (30)$$

where $\mathbf{w}^p$ are the amplitude components for the atom at site p in the 1D lattice, with $p=0$ indexing the atom that interacts with the semi-infinite lattice through the bond stiffnesses $\mathbf{S}_c$, and with p decreasing along the negative z direction. Combining Eqs. (30) and (26) relates the displacements in the semi-infinite lattice to those in the 1D lattice,

$$\mathbf{u}^{0,0,0} = (\mathbf{I} + \mathbf{GS}_c)^{-1} \mathbf{GS}_c \mathbf{w}^0, \quad (31)$$

which allows the influence of the semi-infinite lattice to be transferred to the dynamics of the atom in the contact of the 1D lattice. Using Eq. (31) to cast the terms containing $\mathbf{u}^{0,0,0}$ in terms of $\mathbf{w}^0$ in the equations of motion for the atom in the contact of the 1D lattice ($p=0$) relates the amplitude components at the $p=0$ and $p=-1$ lattice sites,

$$0 = \mathbf{S}_{\text{eff}}\mathbf{w}^0 + \mathbf{S}_1\mathbf{w}^{-1}, \tag{32}$$

where

$$\mathbf{S}_{\text{eff}} = [\mathbf{S}_c(\mathbf{I} + \mathbf{G}\mathbf{S}_c)^{-1}\mathbf{G}\mathbf{S}_c + M_1\omega^2\mathbf{I} - \mathbf{S}_1 - \mathbf{S}_c],$$
$$\mathbf{S}_1 = \begin{bmatrix} K_1^s & & \\ & K_1^s & \\ & & K_1^a \end{bmatrix}, \tag{33}$$

and which ultimately enables the incident phonon amplitudes to be related to the reflected amplitudes in the 1D lattice and the evaluation of the energy transmission coefficient for the contact.

Derivation of the bulk equations of motion for the 1D harmonic lattice is standard in most introductory solid-state texts.[38] Solutions to the 1D lattice dynamics yield longitudinal and transverse oscillations that are decoupled with the following two dispersion relations relating ω, q_l, and q_t for the two polarizations,

$$M_1\omega^2 = 4K_1^a \sin^2(q_l d_1/2), \tag{34}$$

$$M_1\omega^2 = 4K_1^s \sin^2(q_t d_1/2), \tag{35}$$

where d_1 is the 1D lattice constant, and q_l and q_t are the longitudinal and transverse wavevectors. Owing to the dynamics of harmonic processes conserving ω, this dispersion relation gives the corresponding longitudinal and transverse modes in the 1D lattice that couple to the modes of frequency ω in the semi-infinite lattice.

In solving Eq. (32), the amplitude components in the 1D lattice are the sum of contributions arising from the incident and reflected modes, and are of the form

$$\mathbf{w}^p = (\Pi_+)^p\mathbf{P} + (\Pi_-)^p\mathbf{r}, \tag{36}$$

where

$$\mathbf{\Pi}_+ = \begin{bmatrix} e^{iq_l d_1} & & \\ & e^{iq_t d_1} & \\ & & e^{iq_l d_1} \end{bmatrix},$$
$$\mathbf{\Pi}_- = \begin{bmatrix} e^{-iq_l d_1} & & \\ & e^{-iq_t d_1} & \\ & & e^{-iq_l d_1} \end{bmatrix},$$
$$\mathbf{P} = \begin{bmatrix} \sin(\theta)\cos(\phi) \\ \sin(\theta)\sin(\phi) \\ \cos(\theta) \end{bmatrix}, \quad \mathbf{r} = \begin{bmatrix} r_x \\ r_y \\ r_z \end{bmatrix}, \tag{37}$$

where $\mathbf{r}$ are the amplitude components of the reflected mode and $\mathbf{P}$ represents the amplitude components of the incident phonon mode with unit amplitude. θ is the angle between the amplitude displacement and z axis and ϕ is the azimuthal angle with respect to the x axis. We note that the wavevectors for the longitudinal and transverse waves, q_l and q_t, are in general different for a given frequency due to the difference in lattice stiffness for motion in the different directions. Substituting Eq. (36) into Eq. (32) yields the reflected components to be

$$\mathbf{r} = -(\mathbf{S}_{\text{eff}} + \mathbf{S}_1\mathbf{\Pi}_+)^{-1}(\mathbf{S}_{\text{eff}} + \mathbf{S}_1\mathbf{\Pi}_-)\mathbf{P}. \tag{38}$$

With these reflected mode amplitudes, we can proceed to calculate the mode transmission coefficient and junction conductance. For small difference in temperature, the thermal conductance for a polarization i across an interface is expressed as[22]

$$\sigma_i(T) = \sum_{q_i>0} \nu_i^+(q_i)\Gamma_i(\omega_{q_i})\hbar\omega_{q_i}\frac{\partial n(\omega_{q_i},T)}{\partial T}, \tag{39}$$

where v_i^+ is the group velocity for modes incident on the interface, $n(\omega_q,T)$ is the Bose distribution for phonon occupation number at temperature T, and $\Gamma_i(\omega_q)$ is the transmission coefficient for the i polarization. Although the calculation of Eq. (39) is based on the properties of the incident modes, this relation accounts for the bidirectional net interface conductance.[22] Because the energy transmission coefficient represents the difference between the incident and total reflected energy, we can express it in terms of the calculated values for the amplitudes, $\mathbf{r}$, of the modes reflected by the junction. Because the longitudinal and transverse projections of incident modes are linearly independent and have different dispersion relations, we will calculate the transmission for these channels separately and add their contributions to find the net conductance. For incident longitudinal ($\perp$) and transverse ($\parallel$) modes, the expressions for the transmission coefficient that produce the proper energy flux when used in Eq. (39) are

$$\Gamma_\perp = 1 - |r_{z\perp}|^2 - \frac{\nu_t}{\nu_l}(|r_{x\perp}|^2 + |r_{y\perp}|^2), \tag{40}$$

$$\Gamma_\parallel = 1 - |r_{x\parallel}|^2 - |r_{y\parallel}|^2 - \frac{\nu_l}{\nu_t}|r_{z\parallel}|^2, \tag{41}$$

where $\mathbf{r}_\perp$ and $\mathbf{r}_\parallel$ are computed using $\mathbf{P}_\perp = (0,0,1)$ and $\mathbf{P}_\parallel = (1,0,0)$ in Eq. (38), respectively. Because of the symmetry of $\mathbf{G}$ under the transformation $x \leftrightarrow y$, $\Gamma_\parallel$ (polarization in the plane of the surface of the semi-infinite lattice) is independent of ϕ. Since no modes can propagate above the mode cutoff frequency, and that the maximum frequency cutoff for transverse modes, $\omega_{\max,t}$, is less than that of longitudinal modes, we set $\Gamma_\parallel\ (\omega > \omega_{\max,t}) = 0$. For the same reason, $r_{x\perp}$ and $r_{y\perp}$ are zero above $\omega_{\max,t}$.

III. RESULTS AND DISCUSSION

We begin by considering an abrupt junction between two materials with identical bulk stiffness parameters, which will emphasize contributions to the junction impedance due solely to the geometric effects and not impedances due to the material mismatch. In this analysis, for representative results, we model a "siliconlike" material where we choose bond stiffnesses parameters that yield the Lamé constants in the continuum limit of the 2D semi-infinite lattice. For the 2D semi-infinite lattice, the four bond parameters defined in Fig. 1 are interrelated to yield the two independent Lamé constants by the relations[23]

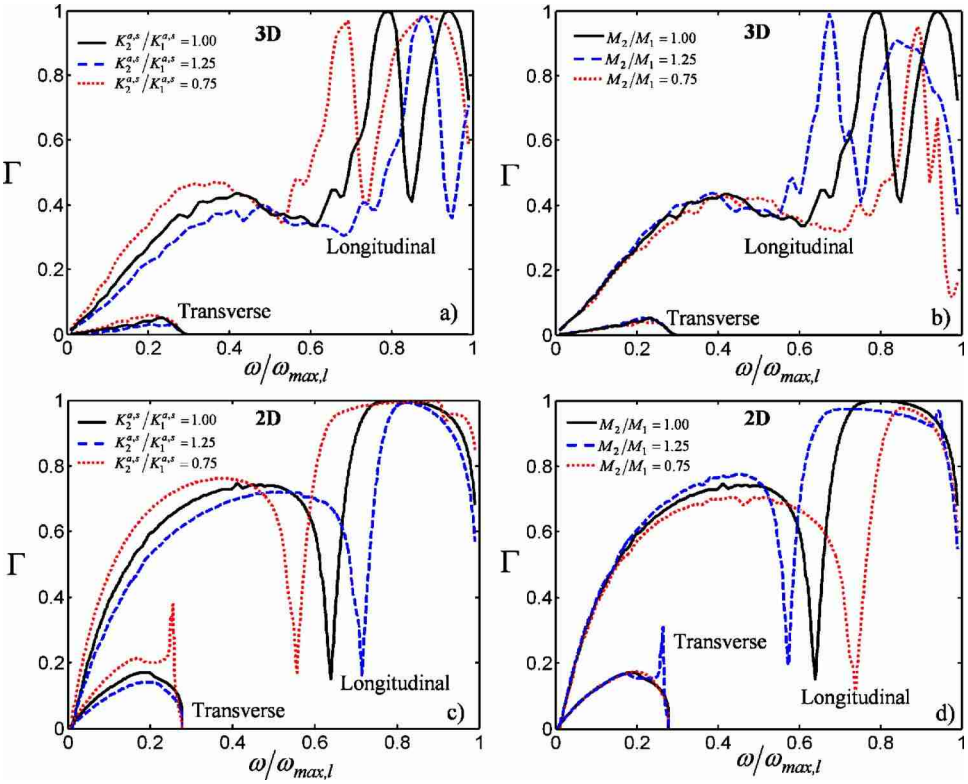

FIG. 2. (Color online) Transmission coefficient for longitudinal and transverse polarizations incident on the junction between the [(a) and (b)] 1D and 3D and [(c) and (d)] 1D and 2D lattices as a function of frequency normalized to the maximum longitudinal polarization of the 1D lattice. The solid black curves show the transmission for lattices with identical stiffness and mass parameters for a siliconlike material. The blue dashed curve and red dotted curve show the impact of changing the ratio of the mass or lattice stiffness parameters in the semi-infinite lattice to those in the 1D lattice to 1.25 and 0.75, respectively. For the 3D case (a) shows the effect of scaling the stiffness and (b) show the effect scaling the mass. For the 2D case, (c) shows the effect of scaling the stiffness and (d) show the effect scaling the mass. The impact of scaling mass and stiffness are qualitatively quite similar, but differ in the details of the transmission curve shapes due to their unique role in the junction boundary conditions.

$$\lambda = \frac{K_2^a - 3K_2^s}{2a_2}, \quad \mu = \frac{K_2^a + K_2^s}{2a_2}, \quad 2K_d^a = K_2^a - K_2^s, \quad K_d^s = 0. \tag{42}$$

For comparison, we used the values of K_2^a and K_2^s derived from Eq. (42) for the semi-infinite fcc lattice. For silicon, we used a lattice constant of a_2=5.4 Å and Lamé constants of λ=56 GPa and μ=79 GPa.[39] Of course, our analysis differs from that of silicon in the basis for the fcc lattice and lattice geometry for the 2D lattice, though we expect the qualitative aspects to be illustrative.

Figure 2 shows the transmission coefficient for longitudinal and transverse modes incident from the 1D lattice into both the 3D fcc lattice [Figs. 2(a) and 2(b)] and 2D square lattice [Figs. 2(c) and 2(d)] as a function of frequency normalized to the maximum frequency of longitudinal mode of the 1D lattice. Figures 2(a) and 2(c) show the impact of changing the relative bond stiffness ratio between the 1D and semi-infinite lattices for the 2D and 3D cases, respectively, while holding all other parameters fixed. Figures 2(b) and 2(d) show the impact of changing the relative mass ratio between the 1D and semi-infinite lattices for the 2D and 3D cases, respectively, while holding all other parameters fixed. The solid black curves are the results for identical parameters in both the 1D and semi-infinite lattices, while the blue dashed and red dotted curves correspond to parameter ratios of 1.25 and 0.75, respectively. To further validate the numerical solution, we performed the calculation in limiting values of the lattice parameters, and in all cases the transmission coefficient behaved appropriately.

The calculation shows that even for identical lattice parameters between the 1D lattice and semi-infinite lattices, the transmission coefficient is less than unity for both polarizations, which is in contrast to the perfect transmission across a junction between identical materials of similar dimensionality. The incomplete transmission across this point junction is due to a change in effective impedance that originates from the strong coupling to modes localized near the surface, which have a different effective stiffness compared to modes in either bulk domain or at the free surface alone. The unity transmission peak demonstrated by both cases indicates that the impedance for modes at these particular frequencies is well matched. That the 3D lattice shows two resonant transmission peaks whereas the 2D lattice shows only one that is due to the modification in the LDOS due to the number of surface waves present in each case, which is related to the surface dimensionality and structure.

Figure 3 shows the evaluation of LDOS [Eq. (29)] for the 3D (black-solid and black-dashed) and 2D (red-solid) lattices for the case of unity parameter ratios, the corresponding transmission coefficients (black dot and black dash-dot), and the bulk density of states of the 1D lattice (red-dashed). The in-plane LDOS is given by the relation $\rho_{\parallel}=(\rho_{xx}+\rho_{yy})/2$ and out of plane is given by $\rho_{\perp}=\rho_{zz}$. A large relative LDOS for a particular mode indicates a relative amplitude enhancement and reduced effective stiffness for that mode. The LDOS of the 3D lattice is on average lower than that of the 2D lattice because, for identical stiffness parameters, the 3D lattice has a large number of neighbor interactions, which increases the effective stiffness of an atom in response to an external force. Comparing the LDOS and transmission in Fig. 3 shows that the transmission peaks and dips are related to peaks in the LDOS caused by the surface modes. The 3D lattice shows two peaks due to the two surface modes for (001) surface of a fcc lattice,[37] whereas the 2D lattice has only one. The large range swept by the spec-

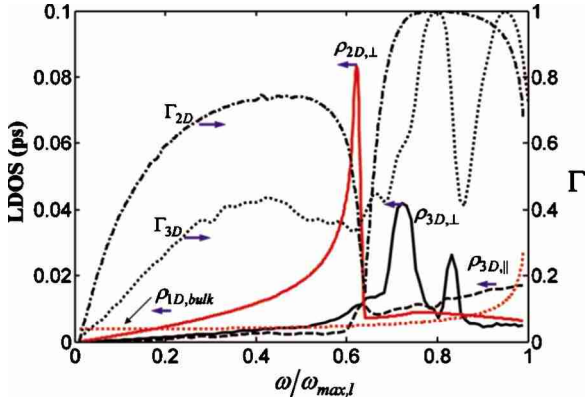

FIG. 3. (Color online) The local density of states for out-of-plane displacements ($\rho_{3D,\perp}$, black solid) for the 3D lattice, in-plane ($\rho_{3D,\parallel}$, black dashed) for the 3D lattice, and out-of-plane ($\rho_{2D,\perp}$ red solid) for the 2D lattice. Also shown is the bulk DOS for the 1D lattice (red solid) and the corresponding transmission coefficients for the 3D and 2D cases. The frequency is normalized to the maximum frequency of the longitudinal mode in the 1D lattice.

tral LDOS due to the surface modes ensures an opportunity for impedance matching between the 1D and semi-infinite lattices, leading to a transmission coefficient of unity. Consequently, the number of transmission peaks depends on the surface dimensionality and number of surface modes present. The peaks in the LDOS tend to reduce the transmission coefficient due to the large density of states mismatch between the lattices. This effect can be understood qualitatively from the fact that a large density of states mismatch is related to a large impedance mismatch due to differing effective mode stiffnesses and velocities. The form of the LDOS in Fig. 3 is a complicated function that deviates, particularly at high frequencies, from the free-surface approximation[40] that is typically employed in calculations, and which is often approximated to scale as a power of the frequency.[18,20] However, the linear trend in the LDOS for the 2D case and quadratic trend for the 3D LDOS (Refs. 37 and 40) observed in Fig. 3 at low frequencies justifies approximating the LDOS as a power of the frequency in this regime. These results indicate that accurate prediction of the energy transmission through abrupt junction requires a rigorous computation of the reservoir dynamics, particularly for the transmission of high frequency modes.

The weak transmission of transverse modes for all cases and frequencies can be explained by the fact that the mode displacement fields in the semi-infinite lattices are mirror symmetric about the z axis, whereas the incident transverse oscillations are antisymmetric with respect to the z axis. This symmetry mismatch causes weak coupling of the two modes. These results are consistent with the calculation by Buldum *et al.*[19] of energy transfer through an atomic wire contacting finite atomic reservoirs, in which transverse modes were found to be highly localized in the wire, weakly coupling to the reservoir modes.

The parameter scaling trends in Fig. 2 show that increasing the stiffness and decreasing the mass ratio between the 1D and semi-infinite lattices show the qualitatively similar effects of shifting the features of the transmission curves up in frequency and decreasing the average transmission coefficient, whereas reducing the ratio shows the opposite trend. The qualitatively similar behavior between increasing the stiffness and decreasing the mass is due to the fact that these parameters enter into the equations of motion for the bulk modes only through their ratio. However, variations in the mass and stiffness of the semi-infinite lattices impact the details of the transmission curves differently due to the fact that they enter differently in the boundary conditions at the lattice junctions. For both semi-infinite lattices at low frequencies, variations in the mass show little impact on the transmission, whereas at high frequencies, particularly for the 3D case, mass variations show a more dramatic change in shape of the transmission peaks. In comparing the effect of varying the stiffness ratio to that of the mass, variations in the stiffness ratio show a greater change in transmission at low frequencies and a less dramatic change in shape of the transmission peaks at higher frequencies, particularly for the 3D case. These differences in trends are related to the larger inertial contribution at higher frequencies. That the change in shape of the transmission curves is a complicated function of the stiffness and mass scaling ratios indicates that the junction transmission arising from material property mismatches are intertwined with the impedance contributions due to geometric effects and do not simply separate into two individual contributions.

The total thermal conductance, including contributions from longitudinal and transverse modes, for the 1D to 2D and 3D cases are shown in Fig. 4. Figure 4(a) shows the impact of variations in the stiffness ratio on the conductance, while Fig. 4(b) shows the impact of variations in the mass ratio. The calculations show that the contribution to the thermal resistance due solely to the geometric effects (solid black curves) is comparable to acoustic mismatch effects at interfaces between materials with similar dimensions. The conductance of the junction with the 3D lattice is less than that with the 2D lattice because of the lower average transmission coefficient resulting from the larger effective stiffness of the 3D lattice. Converting the conductance of 130 pW K^{-1} for the 2D case and 72 pW K^{-1} for the 3D case at 300 K to a thermal resistance using the circular cross-sectional area of the 1D lattice with a diameter of the lattice spacing, i.e., $A_c=\pi(d_1/2)^2$, gives a thermal resistance of 1.8 m^2 K/GW (2D) and 3.3 m^2 K/GW (3D), which is comparable to typical contributions from an acoustic impedance mismatch. From Fig. 2, the transmission coefficient is linear in ω at low frequencies for both semi-infinite lattices, indicating that the low temperature conductance should scale as $\sim T^2$, as is seen in the low temperature limit of Fig. 4. The results do not show any crossing of the conductance trends over the full temperature range.

In the case of an abrupt junction, the largest junction thermal conductance does not occur with materials of similar bulk impedances, as is the case with conventional interfaces between materials of similar dimensionality, but with a semi-infinite lattice that has a stiffness less than or a mass greater than the 1D lattice. Figure 5 shows the junction conductance as a function of the stiffness and mass scaling ratio between the 1D lattice and 3D lattice for 300 and 30 K. For each data set, either the stiffness or mass ratio is varied while all other parameters are held fixed. For 300 K, the results show that

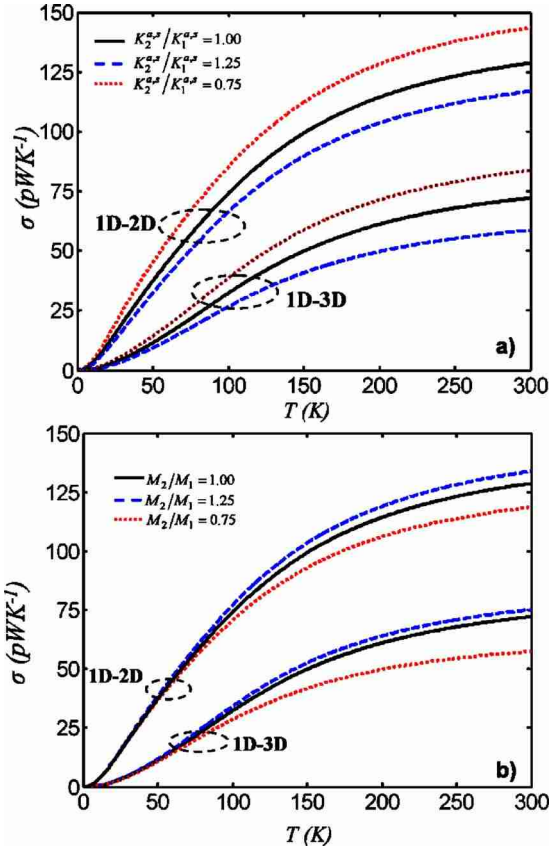

FIG. 4. (Color online) Total thermal conductance as a function of temperature for a junction for both the 3D and 2D cases. (a) shows the impact of varying the stiffness scaling of the semi-infinite lattices or the junction conductance, and (b) shows the impact of varying the mass on the junction conductance. The solid black curves show the transmission for lattices with identical stiffness and mass parameters. The blue dashed curve and red dotted curve show the impact of changing the ratio of the mass or lattice stiffness parameters in the semi-infinite lattice to those in the 1D lattice to 1.25 and 0.75, respectively. The results show that there is a finite conductance of comparable magnitude to the acoustic mismatch conductance even for materials of identical stiffness parameters.

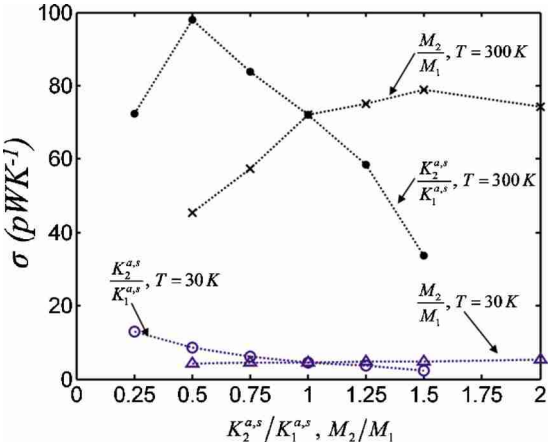

FIG. 5. (Color online) The junction conductance as a function of stiffness ratios between the semi-infinite and 1D lattice at 300 K (black-solid circles) and 30 K (blue open circles) and mass ratios between the semi-infinite and 1D lattice at 300 K (black x) and 30 K (blue triangle). For each data set, the noted ratio is varied while all other parameters are held fixed. The results show that there is a maximum conductance for a for a stiffness ratio of ~0.5 and mass ratio of ~1.5. The conductances at 30 K do not show a maximum conductance.

the maximum thermal conductance of the junction occurs with a stiffness ratio of ~0.5 and a mass ratio of ~1.5. At 30 K, the data do not show a maximum conductance, which is due only to the low frequency phonon modes being populated and the monotonic dependence of the transmission coefficient on the stiffness and mass at low frequencies. These results suggest the thermal conductance of nanostructured thermal interfaces may in general be best optimized by engineering a junction with a reservoir material that has a bulk impedance which is lower than that of the nanostructure, rather than materials that have similar intrinsic impedances. While this lattice dynamics calculation focuses on the relatively simple model problem of a 1D atomic lattice in contact with 2D and 3D semi-infinite lattices, it enables qualitative arguments about the practical phonon transmission effects on contact resistances that will be found in actual nanostructure geometries.

For the interface between a graphene nanosheet and 3D semi-infinite medium, the phonon transmission would be complicated by nonorthogonal lattice geometry in the graphene layer and phonon modes with angular incidence, which each have displacement components in and out of the plane of the interface. We expect that the results of the calculation for the 1D to 2D case would give reasonable predictions for the transmission of longitudinal modes in the graphene sheet with normal incidence. We expect the transmission of normal incidence in-plane and out-of-plane transverse modes to couple weakly to a semi-infinite medium, for reasons similar to those for the weak coupling of transverse modes of the 1D-2D junction. For modes with angular incidence, the energy transmission would be dominated by the transmission of the longitudinal projection of the displacement field, and thus the conductance should scale as $\sim\cos^2(\theta)$, where θ is the angle between the polarization vector and the z axis.

For phonon modes with quadratic dispersion, such as flexure modes in nanotubes,[41] nanowires, and elastic bridges,[25] the amplitude displacement is predominantly parallel to the free interface for the 3D case and for the in-plane mode in the 2D case. Since the quadratic nature of the dispersion relation for these modes is unrelated to the fundamental symmetry basis for the weak coupling of the transverse displacement fields, it has little impact on the transmission since the dispersion relation only enters into the transmission calculation through $q_t(\omega)$ in Eq. (37) for the 1D to 3D and 1D to in-plane-polarized 2D cases. Though these modes are not present in the 1D lattice model used in this analysis, and their detailed calculation is beyond the scope of this work, we investigated the impact of a quadratic dispersion with a simple approximation that modifies the dispersion relation used in Eq. (37) from Eq. (35) to

$$q_t = \frac{\pi}{a_1}\sqrt{\frac{\omega}{\omega_{\max,t}}}. \tag{43}$$

This substitution slightly sharpens the peak in the transverse transmission curve in Fig. 2, with insignificant impact on longitudinal modes, increase in net transmission, and overall impact. Since it is a less common geometry, the transmission

of out-of-plane flexure modes for the 1D-2D case was not considered in this analysis. However, we expect that these flexure modes would couple to the out-of-plane modes with quadratic dispersion in the 2D domain, and that due to similar symmetry arguments, the transmission would behave much like the longitudinal branch with a different effective stiffness.

For the contact between a carbon nanotube and semi-infinite 3D media, we believe that the 1D-3D case is a representative model that suggests that the longitudinal mode will dominate the transmission, while the transverse and torsion modes will have negligible transmission due the large amplitude component in the plane of the interface. The specific form of the phonon transmission function, particularly at high frequencies, would require detailed calculation and be sensitive to the specific interface bonding geometry, including bonding of the nanostructure to multiple atoms on the surface. For materials with polyatomic cross-sectional structure such as multiwalled carbon nanotubes or silicon nanopillars, we expect that as the cross-sectional area increases, the impedance mismatch effects arising from geometry will decrease, and the transmission of modes with wavelength less than the characteristic cross-section dimension will increase due to the stronger coupling to bulklike modes.

Because dimensionally mismatched interfaces are becoming more prevalent in nanostructured technology, their impact on thermal transport investigated by this work strongly motivates the need to consider more detailed calculations considering dimensional mismatched effects.

IV. CONCLUSION

This work uses a lattice dynamics approach to investigate the transmission of energy across an abrupt junction between a harmonic 1D and a 3D fcc lattice and between a 1D and a 2D square lattice with second nearest-neighbor interactions. Although this is a relatively simple geometry compared to many of the practical problems in nanostructures, it provides a simple approximation to nanoscale point contacts and can be viewed as an approximation relevant to nanotubelike structures. The results show that energy strongly couples to modes localized near the surface of the semi-infinite lattice and that the energy transmission coefficient across the interface is less than unity even for identical bulk properties in both domains. The calculation shows that the transmission coefficient for the transverse incident modes is very low at all frequencies due to the symmetry effects. The abrupt change in geometry of the junction presents a thermal resistance contribution that is comparable to that of a mismatch in material impedance. The results suggest that energy transmission through nanoscale thermal interfaces may be enhanced by intentionally using materials with intrinsic impedance mismatches. The lattice dynamics calculations performed here provide an initial perspective on the impact of localized phonon modes on the acoustic mismatch resistance and lay the groundwork for more detailed studies involving 3D molecular dynamics.

ACKNOWLEDGMENTS

M.P. would like to thank the Stanford Graduate Fellowship program, as well as the SRC through Contract No. 2006-KJ-1392 and MARCO IFC through Contract No. GIT B-12-M06-S1.

[1]Z. Huang, F. Chen, R. D'Agosta, P. A. Bennett, M. Di Ventra, and N. Tao, Nat. Nanotechnol. **2**, 698 (2007).
[2]K. Schwab, E. A. Henriksen, J. M. Worlock, and M. L. Roukes, Nature (London) **404**, 974 (2000).
[3]E. Pop, D. Mann, J. Cao, Q. Wang, K. Goodson, and H. Dai, Phys. Rev. Lett. **95**, 155505 (2005).
[4]P. Kim, L. Shi, A. Majumdar, and P. L. McEuen, Phys. Rev. Lett. **87**, 215502 (2001).
[5]M. Fujii, X. Zhang, H. Xie, H. Ago, K. Takahashi, T. Ikuta, H. Abe, and T. Shimizu, Phys. Rev. Lett. **95**, 065502 (2005).
[6]C. W. Chang, D. Okawa, A. Majumdar, and A. Zettl, Science **314**, 1121 (2006).
[7]T. Tong, Y. Zhao, L. Delzeit, A. Kashani, M. Meyyappan, and A. Majumdar, IEEE Trans. Compon. Packag. Technol. **30**, 92 (2007).
[8]M. Panzer, G. Zhang, D. Mann, X. Hu, E. Pop, H. Dai, and K. E. Goodson, J. Heat Transfer **130**, 52401 (2008).
[9]A. Feher, A. A. Mamalui, A. Y. Dul'fan, E. S. Syrkin, and A. G. Shkorbatov, Low Temp. Phys. **31**, 921 (2005).
[10]A. G. Shkorbatov, X. Stef, P. Nyi, E. Bystrenov, and A. Feher, J. Phys.: Condens. Matter **10**, 8313 (1998).
[11]A. G. Shkorbatov, T. Z. Sarkisyants, A. Feher, and P. Stefanyi, Low Temp. Phys. **19**, 881 (1993).
[12]D. E. Angelescu, M. C. Cross, and M. L. Roukes, Superlattices Microstruct. **23**, 673 (1998).
[13]M. C. Cross and R. Lifshitz, Phys. Rev. B **64**, 085324–1 (2001).
[14]W.-X. Li, T. Liu, and C. Liu, Appl. Phys. Lett. **89**, 163104–1 (2006).
[15]C.-M. Chang and M. R. Geller, Phys. Rev. B **71**, 125304–1 (2005).
[16]Y. Ohtsubot, N. Nishiguchit, and T. Sakumaf, J. Phys.: Condens. Matter **6**, 3013 (1994).
[17]A. Ozpineci and S. Ciraci, Phys. Rev. B **63**, 125415–1 (2001).
[18]K. R. Patton and M. R. Geller, Phys. Rev. B **64**, 155320–1 (2001).
[19]A. Buldum, S. Ciraci, and C. Y. Fong, J. Phys.: Condens. Matter **12**, 3349 (2000).
[20]N. Mingo, Phys. Rev. B **74**, 125402–1 (2006).
[21]M. E. Lumpkin, W. M. Saslow, and W. M. Visscher, Phys. Rev. B **17**, 4295 (1978).
[22]D. A. Young and H. J. Maris, Phys. Rev. B **40**, 3685 (1989).
[23]A. S. J. Suiker, A. V. Metrikine, and R. De Borst, J. Sound Vib. **240**, 1 (2001).
[24]T. E. Feuchtwang, Phys. Rev. **155**, 731 (1967).
[25]L. D. Landau and E. M. Lifshitz, *Theory of Elasticity* (Pergamon, New York, 1986).
[26]H. Lamb, Proc. R. Soc. London **72**, 128 (1903).
[27]G. F. Miller and H. Pursey, Proc. R. Soc. London, Ser. A **223**, 521 (1954).
[28]G. F. Miller and H. Pursey, Proc. R. Soc. London, Ser. A **233**, 55 (1955).
[29]T. J. Roystona, H. A. Mansy, and R. H. Sandler, J. Acoust. Soc. Am. **106**, 3678 (1999).
[30]W. M. Ewing, W. S. Jaretzky, and R. Press, *Elastic Waves in Layered Media* (McGraw-Hill, New York, 1962).
[31]D. C. Gazis and R. F. Wallis, J. Math. Phys. **3**, 190 (1962).
[32]A. M. Kosevich and S. E. Savotchenko, Low Temp. Phys. **24**, 748 (1998).
[33]T. E. Feuchtwang, Phys. Rev. **155**, 715 (1967).
[34]D. C. Gazis and R. Herman, Phys. Rev. **119**, 533 (1960).
[35]S. Datta, *Quantum Transport: Atom to Transistor* (Cambridge University Press, New York, 2005).
[36]W. Zhang, T. Fisher, and N. Mingo, Numer. Heat Transfer, Part B **51**, 333 (2007).
[37]M. C. Deshonqueres and D. Spanjaard, *Concepts in Surface Physics* (Springer-Verlag, Berlin, 1993).
[38]N. W. Ashcroft and N. D. Mermin, *Solid State Physics* (Thomas Learning, Inc., Philadelphia, 1976).
[39]W. C. O'Mara, R. B. Herring, and L. P. Hunt, *Handbook of Semiconductor Silicon Technology* (William Andrew, Salem, MA/Noyes, Park Ridge, NJ 1990).
[40]M. R. Geller, Phys. Rev. B **70**, 205421–6 (2004).
[41]G. D. Mahan and G. S. Jeon, Phys. Rev. B **70**, 075405–11 (2004).